Calibration of SeaWiFS. I. Direct techniques

Robert A. Barnes, Robert E. Eplee, Jr., G. Michael Schmidt, Frederick S. Patt, and Charles R. McClain

We present an overview of the calibration of the Sea-viewing Wide Field-of View Sensor (SeaWiFS) from its performance verification at the manufacturer's facility to the completion of its third year of on-orbit measurements. These calibration procedures have three principal parts: a prelaunch radiometric calibration that is traceable to the National Institute of Standards and Technology; the Transfer-to-Orbit Experiment, a set of measurements that determine changes in the instrument's calibration from its manufacture to the start of on-orbit operations; and measurements of the sun and the moon to determine radiometric changes on orbit. To our knowledge, SeaWiFS is the only instrument that uses routine lunar measurements to determine changes in its radiometric sensitivity. On the basis of these methods, the overall uncertainty in the SeaWiFS top-of-the-atmosphere radiances is estimated to be 4–5%. We also show the results of comparison campaigns with aircraft- and ground-based measurements, plus the results of an experiment, called the Southern Ocean Band 8 Gain Study. These results are used to check the calibration of the SeaWiFS bands. To date, they have not been used to change the instrument's prelaunch calibration coefficients. In addition to these procedures, SeaWiFS is a vicariously calibrated instrument for ocean-color measurements. In the vicarious calibration of the SeaWiFS visible bands, the calibration coefficients are modified to force agreement with surface truth measurements from the Marine Optical Buoy, which is moored off the Hawaiian Island of Lanai. This vicarious calibration is described in a companion paper.

OCIS codes: 120.0120, 120.5630, 120.0280, 300.0300, 300.6550, 300.6340.

1. Introduction

The Sea-viewing Wide Field-of-view Sensor (SeaWiFS) is a second-generation ocean-color instrument. As such, its mission has been designed, in large part, from the lessons learned from its predecessor, the Coastal Zone Color Scanner (CZCS).[1] One of the most important lessons was the need for a continuous, comprehensive, calibration-evaluation activity throughout the mission.[2,3] The processing of the CZCS data set was complicated by the degradation of the scanner's radiometric sensitivity, particularly in the visible bands. Although the CZCS had internal lamps, they did not illuminate the entire optical train of the instrument.[4] Therefore changes in the characteristics of the optical components at the input aperture of the scanner could not be determined by measurements of the calibration lamps by the sensor. In addition, it was difficult to separate changes in the sensitivity of the sensor from changes in the outputs from the lamps. To account for these shortcomings, Gordon[5] recommended frequent measurements of the moon or the Sun to determine instrument changes. These two sources fill the input aperture of the instrument plus all of the elements of the optical train. Thus the SeaWiFS mission has been designed to accommodate both lunar and solar measurements.[6]

The original calibration plan for SeaWiFS[3] includes the prelaunch characterization and calibration of the radiometer, plus solar and lunar measurements on orbit to monitor instrument changes, along with comparisons with ships and buoys to check the quality of the onboard calibration. However, with the review of the CZCS calibration by Evans and Gordon,[4] it has become clear that onboard calibration techniques alone are not sufficient to provide good ocean-color measurements. This is due to the accuracy requirements for the measurements. In the visible, the majority of the light flux at the top of the atmosphere (90% or so) comes from the atmosphere itself. Since the removal of the atmospheric radiance from that measured at the top of the atmo-

R. A. Barnes (rbarnes@seawifs.gsfc.nasa.gov), R. E. Eplee, Jr., G. M. Schmidt, and F. S. Patt are with the Science Applications International Corporation, Beltsville, Maryland 20705. C. R. McClain is with the Office for Global Carbon Studies, Laboratory for Hydrospheric Processes, National Aeronautics and Space Administration, Goddard Space Flight Center, Greenbelt, Maryland 20771.

Received 24 October 2000.
0003-6935/01/366682-19$15.00/0

Table 1. SeaWiFS Center Wavelength[a]

SeaWiFS Band	Center Wavelength (nm)
1	412
2	443
3	490
4	510
5	555
6	670
7	765
8	865

[a]These are the nominal center wavelengths from the SeaWiFS specifications.[7] The actual center wavelengths for measurements on orbit are within approximately 1–2 nm of these wavelengths.

sphere is an essential part of ocean-color processing, the radiance from the ocean is calculated as the small difference between two large values. So, an error of 1% in the top-of-the-atmosphere radiance can cause an error of 10% in the derived upwelling radiance at the ocean surface. As a result, for ocean-color measurements, SeaWiFS is a vicariously calibrated instrument. It is the "instrument/atmospheric-correction algorithm system"[4] that is calibrated, since both contribute to the determination of the water-leaving radiance at the ocean surface.

The adoption of a vicarious calibration of SeaWiFS does not preclude the elements in the original calibration plan, which we call the direct calibration of the instrument. The direct calibration of SeaWiFS exists independently of the vicarious calibration, and it is an evolving process. It is different from the calibration in place at the start of the mission, since a great deal has been learned about the operation of the instrument since then. We anticipate that this evolution will continue.

2. Instrument Description

SeaWiFS is an eight-band filter radiometer that is designed to monitor Earth-exiting radiances from ocean scenes. The nominal center wavelengths for the SeaWiFS bands are given in Table 1. The sensor's instantaneous field of view is 1.6 mrad by 1.6 mrad per pixel, with one scan covering 58.3° on either side of nadir. From a measurement altitude of 705 km, this gives Earth measurements, at nadir, that are 1.1 km on a side. SeaWiFS can be set to +20°, 0°, or −20° from nadir in the direction of flight to minimize the effects of ocean glint on the data. Each measurement is digitized to 10 bits, with a typical signal level of 600 digital numbers (DN) and a noise of 1 DN or less. The results of the prelaunch characterization of SeaWiFS are summarized in Barnes *et al.*[7]

SeaWiFS consists of a scanner, which contains the optics, detectors, preamplifiers, and scan mechanisms; and the electronics module, which contains the signal conditioning, command and telemetry, and power supply electronics. The SeaWiFS scanner is illustrated in Fig. 1. Light first strikes the primary mirror, an off-axis parabola, and then is reflected

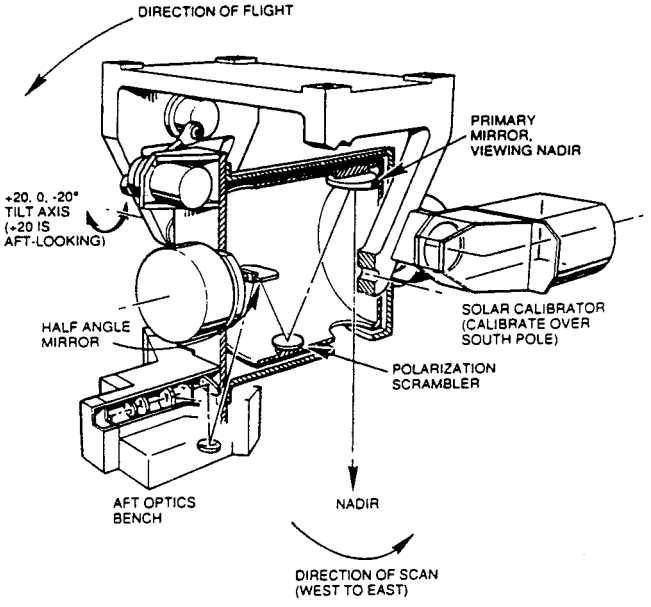

Fig. 1. SeaWiFS scanner assembly. The scanner mounts to the spacecraft with use of the four mounting points at the top of the figure.

from a second-surface polarization scrambler and from the half-angle mirror before reaching the field stop. The primary mirror and the polarization scrambler are mounted on a cylinder that rotates six times per second. The telescope mirror and the entrance aperture on the cylinder have a diameter of 10 cm. The half-angle mirror removes the rotation of the image from the scan of the telescope. It rotates at exactly half the rate of the telescope and polarization scrambler and uses alternating sides on successive telescope scans. The field stop, located at the entrance to the aft optics, is 50% larger than the detectors and restricts light through the system. After the field stop, the light is collimated by another off-axis paraboloid and directed to the aft optics assembly. Dichroic beam splitters in the aft optics divert the light into four focal-plane assemblies, each containing two spectral bands delineated by narrow-band interference filters in close proximity to the detectors. The measurements from the eight bands are acquired simultaneously and are coregistered on the Earth's surface to within one-half pixel.[7]

Attention in the design of SeaWiFS was given to minimizing the sensitivity of the instrument to polarized light. This consideration is the principal reason for splitting the telescope into two sections, each rotating at a different speed. This design has minimized the incidence angle of light on the mirrors. In addition, the use of a polarization scrambler in the fore optics has eliminated the need for individual scramblers to remove residual polarization at each focal-plane assembly.

Two instrument bands, each with four detectors aligned in the scan direction, form a focal plane. Consequently, a point on the ground is seen successively by the four detectors. The outputs from the

four detectors in each band are added using a time-delay-and-integration (tdi) technique to improve the signal-to-noise ratios. The signal from each detector is amplified, processed through a selectable gain stage, and digitized with a 12-bit analog-to-digital converter. The four digital outputs from a band are appropriately delayed, summed to obtain the digital-to-noise advantage, truncated to ten bits, and transmitted to the ground by the Orbview-2 spacecraft. The use of tdi has improved the signal-to-noise ratios of the SeaWiFS measurements by approximately a factor of two. It is used in place of electronic averaging devices, such as integrating capacitors, which also serve to improve signal-to-noise ratios. In addition, this design feature has been used to give SeaWiFS the ability to make measurements of land and bright clouds, in addition to measurements of the oceans, which are significantly darker scenes. The tdi technique is an intrinsic part of the laboratory calibration of the instrument, and a further discussion, along with bilinear gains, is given in Section 3.A. Additional details on the design of SeaWiFS are given in Barnes and Holmes.[8]

3. Direct Calibration

The radiometric model for SeaWiFS is designed to incorporate the laboratory calibration of the instrument with on-orbit changes over time. Thus, for measurements on orbit, the top-of-the-atmosphere radiance $[L_T(\lambda)]$ that is measured by each SeaWiFS band is given by

$$L_T(\lambda) = (\mathrm{DN} - \mathrm{DN}_0)\{k_2(g)\alpha(t_0)[\beta + \gamma(t - t_0) + \delta(t - t_0)^2]^{-1}\}, \quad (1)$$

where λ is the wavelength of the band (in nanometers); DN is the SeaWiFS signal (in digital numbers); DN_0 is the signal in the dark; $k_2(g)$ is the prelaunch calibration coefficient (in mW cm^{-2} sr^{-1} $\mu\mathrm{m}^{-1}$ DN^{-1}); g is the electronic gain; $\alpha(t_0)$ is a vicarious correction (dimensionless) to the laboratory calibration on the first day of on-orbit operations (t_0), and the coefficients β (dimensionless), γ (in day^{-1}), and δ (in day^{-2}) are used to calculate the change in radiometric sensitivity for the band at a given number of days (t–t_0) after the start of operations. For each scan by SeaWiFS, DN_0 is measured as the telescope views the black interior of the instrument. For SeaWiFS, the start of operations (t_0) is the day of the first Earth image, which occurred on 4 September 1997. The determination of the vicarious corrections is explained in a companion paper.[9] To date, there has been no sign of a time dependence in the vicarious calibrations of SeaWiFS. The radiometric changes in the instrument on orbit seem to be adequately modeled by the β, γ, and δ terms in Eq. (1). For this reason, $\alpha(t_0)$ is independent of time. Strictly speaking, the changes in the radiometric sensitivity for each band are not tracked on orbit with use of a single quadratic curve, as is shown in Eq. (1). The actual curves are combinations of linear and quadratic curves pieced together. However, the addition of these features to Eq. (1) makes the equation overly cumbersome for this paper.

A. Laboratory Calibration

For each SeaWiFS band, the calibration coefficient is determined from prelaunch laboratory measurements. The performance specifications for SeaWiFS require a laboratory determination of each calibration coefficient to within 5%.[7] Each coefficient is given as a radiometric sensitivity; that is, it has the units of band-averaged spectral radiance per digital number from the instrument:

$$k_2(g) = \frac{L_B}{(\mathrm{DN} - \mathrm{DN}_0)} = \frac{\left(\dfrac{\int_{\lambda_1}^{\lambda_2} L_\lambda R_\lambda \mathrm{d}\lambda}{\int_{\lambda_1}^{\lambda_2} R_\lambda \mathrm{d}\lambda}\right)}{(\mathrm{DN} - \mathrm{DN}_0)}, \quad (2)$$

where the band-averaged spectral radiance is L_B (in mW cm^{-2} sr^{-1} $\mu\mathrm{m}^{-1}$). The ratio of integrals in the equation provides the definition of the band-averaged spectral radiance: L_λ is the spectral radiance from the source (in mW cm^{-2} sr^{-1} $\mu\mathrm{m}^{-1}$) at wavelength λ; R_λ is the spectral response for the band; and λ_1 and λ_2 are the lower and upper limits of integration. These wavelengths mark the range for which the band has a significant spectral response. For each SeaWiFS band, these limits are 380 nm and 1150 nm.[10]

In addition to the spectral responses, the laboratory calibration of SeaWiFS uses the output of a large aperture-integrating sphere to provide a calibrated radiance over the area of the aperture and over the wavelength interval from λ_1 to λ_2. For the solution of the equation, the calibration values[11] are provided as a set of spectral radiances L_λ at each wavelength in the spectral response of the band. The resulting pairs of sphere spectral radiances and band spectral responses are used to calculate L_B by way of the ratio of integrals in Eq. (2).

For SeaWiFS, there were two laboratory calibrations, one in California by the instrument manufacturer (Hughes Santa Barbara Research Center, now Raytheon Santa Barbara Research Center) in 1993,[12,13] and one in 1997 at the facility of the spacecraft manufacturer (Orbital Sciences Corporation) in Maryland. The 1997 calibration[11] was performed by scientists from National Institute of Standards and Technology (NIST) and from the SeaWiFS Project. For the 1993 calibration by the instrument manufacturer, the spectral radiances from the integrating sphere were determined with use of a quartz halogen lamp that had an irradiance calibration traceable to NIST. The irradiance from the lamp was converted to radiance with use of a diffuse reflecting plaque that had a surface of pressed halon. The material for the surface was supplied by NIST as a standard reference material, along with instructions for the fabrication of the plaque surface. The spectral radiances from the integrating sphere were determined from com-

parisons with the spectral radiances from the plaque and with use of a transfer radiometer designed and built by the instrument manufacturer.

For the 1997 calibration at the facility of the spacecraft manufacturer, the calibration radiances were provided by an integrating sphere from the NASA Goddard Space Flight Center. The calibration and characterization of the Goddard sphere was performed at NIST in 1995.[14] The calibration standard was a gas-filled tungsten ribbon lamp that was itself calibrated for spectral radiance at the Facility for Automated Spectroradiometric Calibrations at NIST. During the 1995 NIST calibration of the sphere, measurements of the sphere spectral radiance were made with use of the SeaWiFS Transfer Radiometer (SXR), which was designed, fabricated, and characterized for the SeaWiFS Project by NIST.[15] For the 1997 calibration of SeaWiFS, measurements of the sphere spectral radiance were repeated with use of the SXR. The differences between the 1995 and 1997 measurements by the SXR were used to determine the changes in the output of the Goddard sphere over that period of time. There is an uncertainty in these changes that comes from the use of the SXR as a transfer radiometer for measurements of the same source over time. This is incorporated into the estimated uncertainties for the calibration.[11]

There is no uncertainty analysis for the 1993 calibration of SeaWiFS. The uncertainties for the 1997 calibration of SeaWiFS range 2–3%, with the greatest uncertainty for the calibration coefficient for band 1 (412 nm). The 1997 calibration of SeaWiFS agrees with the initial 1993 calibration to within 4%. If it is assumed that the uncertainties from the 1993 calibration are comparable with those from 1997, then the uncertainties for the two calibrations overlap.

The calibration coefficients from the 1997 SeaWiFS calibration are the official prelaunch coefficients for SeaWiFS. They are shown in Fig. 2. They are the coefficients for the standard SeaWiFS gain (gain 1). There are three other SeaWiFS gains: gain 2, which is used for measurements of low-light levels from the Earth; and gains 3 and 4, which are used for lunar and solar diffuser measurements. For each channel, a remotely commanded variable-gain amplifier located after the photodiode and its transimpedance amplifier is used to change the channel's output, depending on the source to be measured. These gains are determined with use of a constant voltage pulse that is fed into the variable gain amplifier when the telescope views the black interior of the instrument and the photodiode output is zero. During this procedure the variable-gain amplifier is cycled through its set of gains, and the output of each channel, relative to gain 1, gives the gain ratio. This test is used on a regular basis to determine changes in the gain ratios on orbit. It was also applied during the 1997 laboratory calibration of SeaWiFS.[11]

As shown in Fig. 2(a), SeaWiFS has 32 channels, with 4 channels per band. Each channel has its own detector, amplifier, and analog-to-digital converter, and each of the 32 channels was calibrated independently before launch.[11] The detector for each channel in each band is located under the same interference filter as the other three[16] so that each channel in a band has the same spectral response. The detectors are located adjacent to each other on the focal plane in the along-scan direction. Thus each channel views the same pixel on the Earth's surface in sequence. When the digital outputs from the channels are summed and divided by four to give the mean, the noise in that mean is approximately a factor of two smaller than the noise from each individual channel. Since the four channels do not measure each spot on the Earth simultaneously, with a delay of about 42 μs between channels,[7] the electronics for each band uses a set of hard-wired shift registers to account for these delays and then uses summing circuits to combine the digital outputs from the channels. This summing technique is tdi. There are many possible combinations of channels to sum for each band. However, the combination that

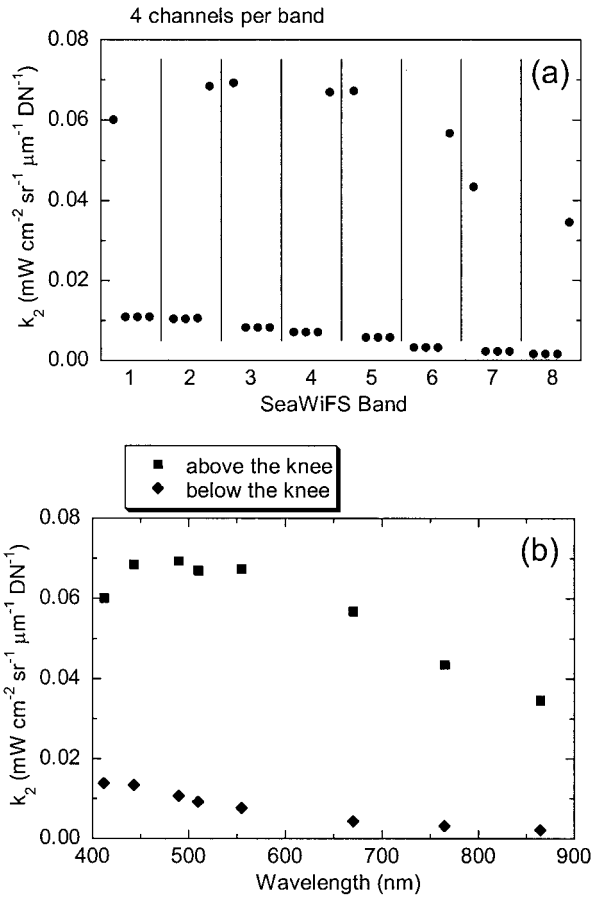

Fig. 2. SeaWiFS calibration coefficients. The coefficients are given as sensitivities, with units of spectral radiance per digital number. (a) Calibration for the individual channels. The low-sensitivity channels were placed on the outside edges of the focal planes to help reduce the effects of stray light in the instrument.[16] (b) Combined calibration coefficients for each band. The bands are presented in terms of their center wavelengths. Below the knee, none of the channels in the band are in digital saturation. Above the knee, all of the high-sensitivity channels are in digital saturation, each with an output of 1023 DN.

minimizes noise in the band's output uses the combination of four channels to produce one output (a tdi of 4:1). This is the standard tdi combination for SeaWiFS. To date, SeaWiFS measurements on orbit have been made with a tdi of only 4:1.

Originally, SeaWiFS was designed with the four channels in each band having the same gain. However, before its delivery, SeaWiFS was modified to ameliorate the effects of stray light in its measurements.[16] Stray light is most severe when the instrument measures the ocean near bright clouds. On the basis of laboratory measurements,[16] a rudimentary stray-light correction algorithm has been developed for SeaWiFS.[17] During the stray light modification of SeaWiFS, it was recognized that, for such an algorithm to work, it is necessary to know the brightness of the clouds (or land surfaces) close to the location that is being measured. As a result, the engineering team at the instrument's manufacturer devised a means of measuring the radiance from the dark ocean surface and the radiances from land and clouds using the same band. This measurement is done with use of bilinear gains and is based on the knowledge that each channel in the instrument will reach digital saturation (1023 DN in a 10-bit system) before its analog circuits saturate.

As a result, each SeaWiFS band now has three high-sensitivity channels (less spectral radiance per digital number) and one low-sensitivity channel (more spectral radiance per digital number), as shown in Fig. 2(a). For a tdi of 4:1, the overall calibration coefficient of a band for a given gain, $k_2(g)$, is a combination of those for the individual channels:

$$\frac{1}{k_2(g)} = \left(\frac{1}{4}\right)\left(\frac{1}{k_2(g,1)} + \frac{1}{k_2(g,2)} + \frac{1}{k_2(g,3)} + \frac{1}{k_2(g,4)}\right), \tag{3}$$

where 1, 2, 3, and 4 denote the channel in the band. The combined calibration coefficients for the SeaWiFS bands are shown in Fig. 2(b). Here the bands are presented in terms of their nominal center wavelengths (see Table 1). The diamonds in Fig. 2(b) denote calibration coefficients when none of the channels are in digital saturation. However, for measurements of bright targets, three of the channels saturate at 1023 DN and provide constant values to the combined output. For these radiances, only the low-sensitivity channel responds to changes in the light level, and $k_2(g)$ becomes the calibration coefficient for that channel, as shown by the squares in Fig. 2(b). This type of instrument setup is called a bilinear gain.

The bilinear gain can also be shown as a calibration curve, which gives the spectral radiance viewed by SeaWiFS in terms of the signal from the instrument. The calibration curve for band 1 (gain 1) is shown in Fig. 3(a), where the slope of each segment is $k_2(g)$. The knee in the bilinear gain occurs at about 800 DN with a radiance of about 11 mW cm^{-2} sr^{-1} μm^{-1}.

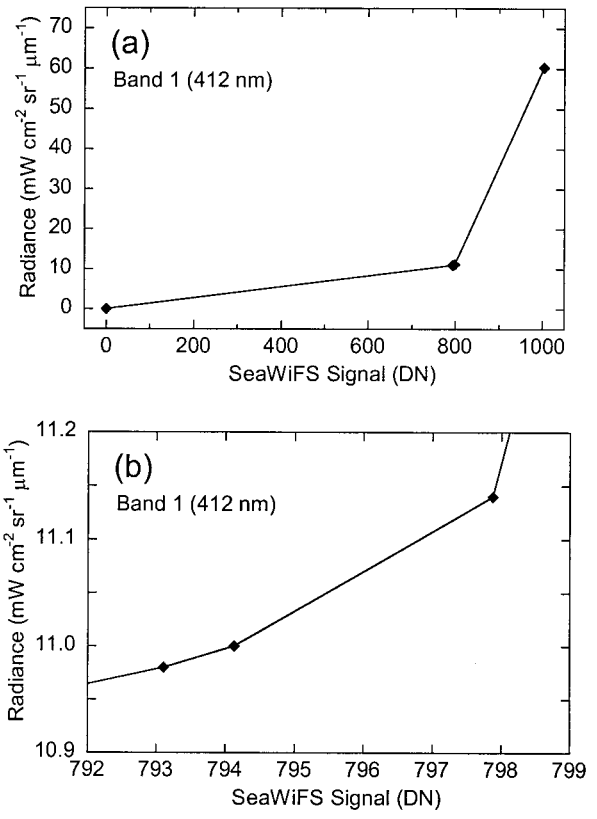

Fig. 3. The bilinear calibration curve for SeaWiFS band 1. The signals are the net outputs from the band (after the zero offset has been removed). (a) Measurements over the entire dynamic range of the band. The spectral radiances for ocean measurements occur below the knee and for land occur above the knee. The knee is actually three knees in one. (b) Measurements in the region of the three knees. Each knee occurs when one of the high-sensitivity channels goes into digital saturation (1023 DN).

However, the three high-sensitivity channels do not saturate at the same radiance, so there are actually three knees in the calibration curve as each of the high-sensitivity channels goes into digital saturation [see Fig. 3(b)]. This setup gives SeaWiFS the capability of measuring dark ocean targets below the knee and bright land and cloud targets above.

B. Transfer-to-Orbit Experiment

For SeaWiFS, the transfer-to-orbit experiment[18] can be used to estimate the change in the radiometric sensitivity of the instrument from the calibration at the manufacturer's facility to the start of on-orbit operations. Alternately, the transfer-to-orbit experiment can be considered to provide uncertainty terms that can be added to those from the laboratory calibration and is the way that the transfer-to-orbit experiment is used here. Thus there is no term in the on-orbit radiometric calibration equation [Eq. (1)] resulting from the transfer-to-orbit experiment. Since an onboard diffuser plate is required for these measurements, the experiment measures changes in the instrument-diffuser system. There is no mecha-

nism in this experiment to separate changes in the diffuser from changes in the instrument.

The concept for the experiment is simple. Measurements of the solar irradiance are made from the ground before launch. Using these measurements, the initial on-orbit response of the instrument, when the solar irradiance is viewed, is predicted. This requires no absolute calibration of the instrument, since the experiment examines the relative changes of the instrument output from the ground to orbit. The experiment hinges primarily on the quality of the atmospheric transmission measurements during the ground portion of the experiment. The effect of the absolute value of the solar irradiance model on this experiment is very small. The instrument views the Sun for both measurements and, to an excellent approximation, the solar irradiance is removed when the ratio of the two measurements is taken.

In addition to two measurements of the sun by SeaWiFS, the transfer-to-orbit experiment requires three additional steps: the alignment of SeaWiFS on the ground to match the on-orbit solar incidence angles for the second measurement; the removal of the effects of diffuse skylight from the ground measurements of the solar irradiance by SeaWiFS; and the measurement of the attenuation of the solar irradiance by the atmosphere during the ground measurements. This is made by a narrow field-of-view solar radiometer that was specifically designed for atmospheric transmittance measurements.

The solar measurements are based on the bidirectional reflectance distribution function (BRDF) of the SeaWiFS diffuser, which is defined in a simplified form[18] at each wavelength as

$$F_\lambda(\phi_I, \theta_I) = \frac{L_\lambda}{E_\lambda \cos(\theta_I)}, \tag{4}$$

where $F_\lambda(\phi_I, \theta_I)$ is the diffuser BRDF (in sr^{-1}) with an azimuthal incidence angle on the diffuser of ϕ_I and a zenith angle of θ_I; L_λ is the spectral radiance from the diffuser; and E_λ is the solar spectral irradiance incident on the diffuser (in mW cm^{-2} μm^{-1}). The incident solar irradiance is calculated from a solar model and the Earth–Sun distance as

$$E_\lambda = \frac{E_{S,\lambda}}{D^2}, \tag{5}$$

where $E_{S,\lambda}$ is the model irradiance at a distance of 1 AU and D is the Earth–Sun distance (in AU). Equations (4) and (5) can be combined and solved for L_λ, yielding

$$L_\lambda = F_\lambda(\phi_I, \theta_I) \frac{E_{S,\lambda}}{D^2} \cos(\theta_I). \tag{6}$$

L_λ from this equation can be substituted into Eq. (2), which can then be solved for the net SeaWiFS signal ($DN - DN_0$), giving

$$(DN - DN_0) = \left[\frac{\cos(\theta_I)}{k_2(g) D^2}\right] \frac{\int_{\lambda_1}^{\lambda_2} F_\lambda(\phi_I, \theta_I) E_{S,\lambda} R_\lambda d\lambda}{\int_{\lambda_1}^{\lambda_2} R_\lambda d\lambda}. \tag{7}$$

Equation (7) gives the net signal from the SeaWiFS band when the solar irradiance is directly measured.

For SeaWiFS, the integrals are calculated as sums from 380 to 1150 nm at 1-nm intervals. Since the values of R_λ are very small at 380 and 1150 nm,[18] a simple summation of histograms is sufficient. For the transfer-to-orbit experiment, the ground-based measurements are designated A and the on-orbit measurements are designated B. This gives the on-orbit equation the form

$$(DN - DN_0)_B = \left[\frac{\cos(\theta_I)_B}{k_2(g_B) D_B^2}\right] \frac{\sum_{\lambda=380}^{1150} F_\lambda(\phi_I, \theta_I) E_{S,\lambda} R_\lambda \Delta\lambda}{\sum_{\lambda=380}^{1150} R_\lambda \Delta\lambda}, \tag{8}$$

where $\Delta\lambda$ is 1 nm. For the ground-based measurements, the equation is nearly the same:

$$(DN - DN_0)_A = \left[\frac{\cos(\theta_I)_A}{k_2(g_A) D_A^2}\right] \frac{\sum_{\lambda=380}^{1150} F_\lambda(\phi_I, \theta_I) E_{S,\lambda} T_\lambda R_\lambda \Delta\lambda}{\sum_{\lambda=380}^{1150} R_\lambda \Delta\lambda}, \tag{9}$$

except for the transmittance of the direct solar beam by the atmosphere, T_λ (dimensionless).

The atmospheric-transmittance spectrum is shown in Fig. 4. The measurements were made with a solar radiometer with 10 bands covering the spectral range from 370 to 1040 nm. The transmittances are lower than are expected for a clean atmosphere due to haze from nearby fires in the Los Angeles basin on the day of the measurement. On the basis of calibrations of the solar radiometer done before and after the transfer-to-orbit experiment, it is expected that the error in the atmospheric transmittances was approximately 3% or less at the measurement wavelengths.[18] Along with the measured barometric pressure at the ground, these transmittances were used to calculate the atmospheric-transmittance spectrum at 1-nm intervals from 380 to 1150 nm, which is the wavelength range of the SeaWiFS spectral-response measurements. The atmospheric transmittance is the major source of uncertainty in the transfer-to-orbit experiment.

For the ground measurements, there was also light from the blue sky illuminating the diffuser. The

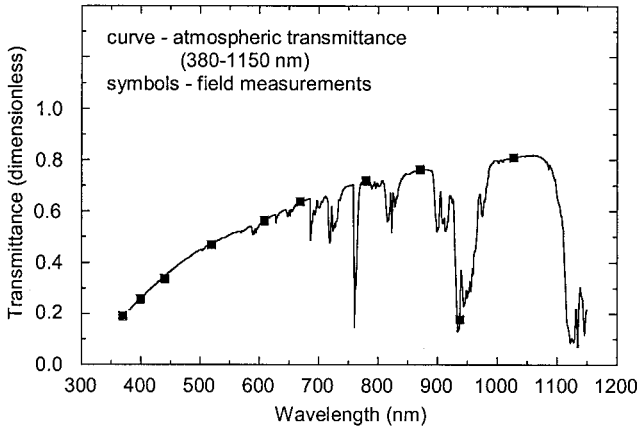

Fig. 4. Atmospheric transmittances during the ground portion of the transfer-to-orbit experiment. The symbols give the measurements from the sun photometer. The curve gives the derived atmospheric transmittance spectrum.

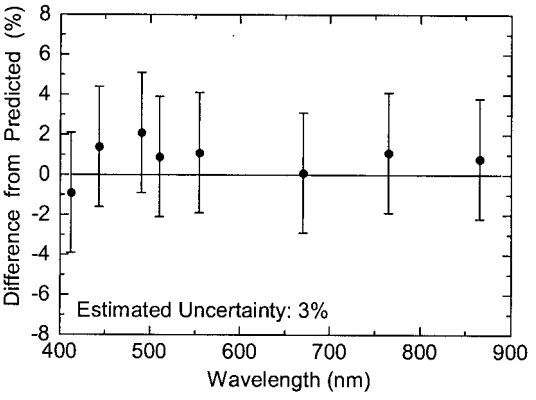

Fig. 5. Results of the transfer-to-orbit experiment for the eight SeaWiFS bands. These are the differences of the on-orbit measurements of the sun from those predicted from the ground measurements prelaunch. At the 3% level, there is no sign of change in the radiometric sensitivity of SeaWiFS from its manufacture to the start of on-orbit operations.

amount of this light was determined through blocking of the direct solar flux by way of a disk supported over the diffuser,[18] allowing an adjustment of the ground-based signals. This adjustment leaves the transmittance of the direct solar beam as the only atmospheric effect necessary for Eq. (9).

The prediction of the net signal on orbit is made with the assumptions that neither the BRDF of the diffuser nor the spectral response of the band changes. In addition, the azimuthal and zenith incidence angles for the solar irradiance during the ground-based measurements were set to duplicate those on orbit, removing the angular dependence. This allows the calculation of the ratio of Eq. (8) to Eq. (9), giving

$$(\mathrm{DN} - \mathrm{DN}_0)_B = \left[\frac{k_2(g_A)}{k_2(g_B)}\right]\left[\frac{D_A^2}{D_B^2}\right] \times \left[\frac{\sum_{\lambda=380}^{1150} F_\lambda(\phi_I, \theta_I) E_{S,\lambda} R_\lambda \Delta\lambda}{\sum_{\lambda=380}^{1150} F_\lambda(\phi_I, \theta_I) E_{S,\lambda} T_\lambda R_\lambda \Delta\lambda}\right] \times (\mathrm{DN} - \mathrm{DN}_0)_A. \quad (10)$$

Except for the calibration coefficient $k_2(g_B)$ used for the diffuser measurements on-orbit and the Earth–Sun distance for the on-orbit measurement D_B^2, Eq. (10) can be evaluated for $(\mathrm{DN} - \mathrm{DN}_0)_B$ by use of prelaunch values. The upper summation in Eq. (10) gives the calculated output for the band's photodiode (in pA) for the measurement on orbit, and the lower summation in the equation gives the calculated output for the measurement on the ground.

SeaWiFS made its first solar measurements 39 days after launch, following a period of orbit raising and instrument outgassing. On day 72, there was a problem with the constants for orbit determination uplinked to the satellite, causing the spacecraft computer to shut down and go into safehold. On day 80, regular solar measurements were started again. Based on the measurements of the sun from day 39 to 72, linear trend lines were used to estimate the fractional change in the solar measurements from the launch date to day 39. These changes ranged from 0.8 to 2.5%.[18]

Figure 5 shows the ratio of the signals from the SeaWiFS bands at the start of the mission to the values predicted from the ground measurements.[18] The mean value for these ratios is 1.008, and the standard deviation is 0.009. The results of the experiment are summarized in Table 2. The SeaWiFS signals at the start of the mission include the correction for changes between the launch date and the start of on-orbit solar measurements. Without the application of this correction, the mean value for the ratios is 0.995 with a standard deviation of 0.012.[18]

There are four uncertainties in the transfer-to-orbit experiment. The first is the uncertainty in the

Table 2. Results of the Transfer-to-Orbit Experiment[a]

SeaWiFS Band	Predicted Signal (DN)	Actual Signal (DN)	Ratio (Actual/Predicted)
1	428.9	525.1	0.991
2	385.1	390.6	1.014
3	451.0	460.5	1.021
4	455.9	460.1	1.009
5	438.9	443.8	1.011
6	380.6	381.0	1.001
7	375.5	379.7	1.011
8	366.0	368.6	1.007
Mean			1.008
Standard deviation			0.009

[a]On the basis of measurements before launch, the signal for solar measurements immediately after launch were predicted. The results as the ratio of the actual measurements to the predicted ones.

atmospheric transmittances for the ground measurements, which is 3%.[18] The second is the uncertainty in the calculation of the amount of diffuse light with use of the occulting disk during the ground measurements, which is estimated at 0.25% of the signals from that part of the experiment. The third is the uncertainty in the diffuser reflectance for the two parts of the experiment. This does not arise from the absolute value for the reflectance but from the difference in the angle of the solar irradiance for the two parts of the experiment. For the ground portion, the alignment was within 0.25° of the normal to the input aperture of the diffuser housing. For the measurements on orbit, the difference was 2°. For the SeaWiFS diffuser, this leads to a change of 0.3% in the BRDF.[19] The fourth uncertainty arises from the correction for the changes in the instrument-diffuser system from the launch of SeaWiFS to the date of the first measurements of the sun. The corrections for these changes are 1–2%. Because an extrapolation is required to determine these changes, the uncertainty in the corrections is estimated to be 1%. For the four uncertainties, the square root of the sum of the squares is 3.2%. However, it is clear that the overall uncertainty is not known at the 0.1% level, so the uncertainty estimate for the experiment is set at 3%, which is the value of the principal uncertainty source. This is the uncertainty used in Fig. 5.

The dependence of the experiment on the atmospheric attenuation measurement can be demonstrated with use of the technique of band averaging, which can be applied to more than radiances. In the SeaWiFS atmospheric-correction algorithm, the band-averaged solar irradiance is used as an input to the calculations.[20,21] In such a manner, the summation in Eq. (9) can be approximated as the product of the band averages of the BRDF, solar irradiance, and atmospheric transmittance,

$$\frac{\sum_{\lambda=380}^{1150} F_\lambda(\phi_I, \theta_I) E_{S,\lambda} T_\lambda R_\lambda \Delta\lambda}{\sum_{\lambda=380}^{1150} R_\lambda \Delta\lambda} \approx \left[\frac{\sum_{\lambda=380}^{1150} F_\lambda(\phi_I, \theta_I) R_\lambda \Delta\lambda}{\sum_{\lambda=380}^{1150} R_\lambda \Delta\lambda}\right]\left[\frac{\sum_{\lambda=380}^{1150} E_{S,\lambda} R_\lambda \Delta\lambda}{\sum_{\lambda=380}^{1150} R_\lambda \Delta\lambda}\right] \times \left[\frac{\sum_{\lambda=380}^{1150} T, R_\lambda \Delta\lambda}{\sum_{\lambda=380}^{1150} R_\lambda \Delta\lambda}\right]. \quad (11)$$

Each term in Eq. (11) can be calculated independently, and each can be treated as a constant. This technique allows a simplification of the ratio of summations that were calculated for Eq. (10) to

$$\frac{\sum_{\lambda=380}^{1150} F_\lambda(\phi_I, \theta_I) E_{S,\lambda} R_\lambda \Delta\lambda}{\sum_{\lambda=380}^{1150} F_\lambda(\phi_I, \theta_I) E_{S,\lambda} T_\lambda R_\lambda \Delta\lambda} \approx \left[\frac{\sum_{\lambda=380}^{1150} T_\lambda R_\lambda \Delta\lambda}{\sum_{\lambda=380}^{1150} R_\lambda \Delta\lambda}\right]^{-1}, \quad (12)$$

where the BRDF and solar-irradiance terms fall out of the ratio. For each of the SeaWiFS bands, the values in the left-hand and right-hand sides of Eq. (12) agree at the 0.2% level or better.[18] As a result, the transfer-to-orbit experiment does not depend on either the absolute value of the diffuser BRDF or the absolute value of the solar irradiance. However, this does not eliminate the need in the experiment for the characterization of the diffuser, since an understanding of the operation of the instrument is fundamental to its use.

C. Lunar Measurements

The analysis of SeaWiFS lunar measurements[22] continues to evolve. In large part, this evolution follows the addition of new measurements to the data set.[6,23] For SeaWiFS, the moon is used as an external diffuser. It reflects sunlight, and SeaWiFS views the radiance from its surface. The members of the SeaWiFS Project do not consider themselves experts on the reflecting properties of the moon. Our understanding of the lunar surface comes almost exclusively from the published literature. However, it has become clear to us that there are limitations in the current models of the moon. One solution to this situation is an updated lunar model. To this end, Hugh Kieffer of the United States Geological Survey in Flagstaff, Arizona, has initiated a program of lunar measurements and the development of a multiwavelength lunar model.[24–26] When operational, this model will give the reflectance of the moon for any viewing geometry from a satellite instrument in Earth orbit. The model will provide the lunar reflectance for 23 bands in the visible and near infrared for approximately 120,000 points in the lunar grid.[25] The resolution of the model is significantly better than that for the lunar measurements by SeaWiFS, in which the diameter of the moon is equivalent to the width of about seven SeaWiFS pixels. However, as of this writing, the United States Geological Survey lunar model is not operational.

For SeaWiFS, the lunar images that are analyzed consist of scenes that are typically 22 samples wide by 33 scan lines long.[6] These scenes include the entire lunar image, plus a small region of black space surrounding the moon. For individual SeaWiFS lunar pixels, the moon overfills the field of view of the instrument, and each individual pixel gives the radiance for a section of the lunar surface. For the lunar scenes, however, the integrated image of the moon is treated as an irradiance, since the apparent area of the lunar disk is a function of the instrument–moon distance. The SeaWiFS lunar analysis accounts for

this factor. In addition, it accounts for the Sun–moon distance, the fraction of the lunar surface that is illuminated during the measurement, and the rotation rate of the spacecraft, which effects the apparent size of the integrated lunar image.[6] Finally, the analysis corrects for changes in the reflectance of the moon as a function of the lunar-phase angle.

1. *Lunar Phase Angle Correction*

Among the changes to the lunar analysis in Barnes *et al*.[6] is the incorporation of a wavelength-dependent modification to the correction for the lunar reflectance with phase angle. The change of the overall reflectance of the lunar surface is non-Lambertian and can be approximated by Hapke's bidirectional reflectance equation.[27] Helfenstein and Veverka[28] used Hapke's equation and a set of empirically derived constants to provide values of disk-integrated reflectance versus phase angle. For the initial analysis of the SeaWiFS lunar measurements,[6] the values from Helfenstein and Veverka[28] were fitted to a quadratic curve over lunar-phase angles from 3° to 11° from full moon, and this curve was applied to each of the SeaWiFS bands.

For the SeaWiFS Project, the uncertainty in the correction for phase angle is a principal consideration in the lunar measurements. Since we are not experts in the characterization of the lunar surface, we have chosen to minimize the phase-angle dependence by measuring the moon at a single phase angle (7° from full phase). Operationally, SeaWiFS makes measurements once per lunar month during the orbit nearest 7° lunar phase. Because SeaWiFS makes about 14 orbits of the Earth per day, it is possible to time each lunar measurement to within about 0.5° of 7° phase. However, other operational requirements, particularly the requirement for at least one orbit between a lunar measurement and a data downlink, have caused some lunar measurements to occur at phase angles that are 2° or more away from the desired angle. The effects of these angular differences have shown up in the SeaWiFS data set.

The analysis of the phase-angle differences and the design of the correction are described in Barnes and McClain.[23] In essence, measurements with phase angles more than 1° from 7° phase were removed from the lunar data set, and the remaining values were fitted to trend lines versus time. This gave a set of reference lines with the outliers removed. The differences of the outliers from the reference lines were calculated, plotted versus phase angle, and fitted to straight lines. The slope of the lines for these outliers provides corrections for each band to the original phase-angle curve.[23] The effects of these corrections are small; however, they significantly reduce the scatter in the data points about the trend lines, especially for data from phase angles more than 1° from the standard 7° phase angle for the measurements.[23]

2. *Normalization to Bands 3 and 4.*

The trends in the SeaWiFS lunar measurements for the visible bands (bands 1 through 6) are shown in Fig. 6. The integrated lunar radiances are normalized for lunar phase angle and for the other geometric factors mentioned above and in Barnes *et al*.[6] In addition, the measurements are normalized to a value of unity for the date of the first lunar measurement (4 November 1997). This puts the data sets for all of the bands onto the same scale. For the SeaWiFS Project, it is called the first normalization. Each panel in Fig. 6 also contains a linear regression line as a visible reference. There is a markedly similar measurement-to-measurement pattern for each band in the figure. We feel that this pattern derives from the effects of lunar libration[6] or possibly from some other external factor for which we have not accounted. We do not feel that the pattern is instrumental in nature, since it is common to all bands.

Figure 7 shows a composite of the measurements shown in Fig. 6. However, the linear regressions have been removed and replaced with a single line that connects the average value for bands 3 and 4 for each measurement. Figure 7 also shows the measurement-to-measurement pattern seen in Fig. 6. In addition, Fig. 7 shows a divergence in the trends for the individual bands. This divergence is also seen in the different regressions lines in the panels of Fig. 6. Among the visible bands, bands 1 and 6 are trending slightly lower than the others, and bands 3 and 4 are trending slightly higher. We know of no mechanism that would cause the radiometric sensitivity of bands 3 and 4 to increase relative to the other bands. The interference filters for the SeaWiFS bands are of similar construction, and the focal planes are of nearly identical design. As a result, we have assumed that the radiometric sensitivities of these bands are decreasing less than the other bands or that they are not changing at all. An improvement in this assumption is not possible, based on our current understanding of the moon. For this reason, we have chosen to normalize the SeaWiFS lunar measurements to the average value for bands 3 and 4 for each measurement. For the SeaWiFS Project, this is called the second normalization. This is the reason that each panel in Figs. 6–8 has the annotation "before second normalization."

The trends in the lunar measurements for SeaWiFS bands 7 and 8 (before the second normalization) are shown in Fig. 8. The changes in these bands are significantly greater than those found in bands 1–6. For this reason, the scaling of Fig. 8 is different from that for Figs. 6 and 7. However, the measurement-to-measurement pattern from Figs. 6 and 7 is also present here.

3. *Lunar Trends*

The changes in the radiometric sensitivity used in Eq. (1) are shown in Fig. 9. The measurements have been normalized to the average value of bands 3 and 4 for each measurement. In addition, the curves

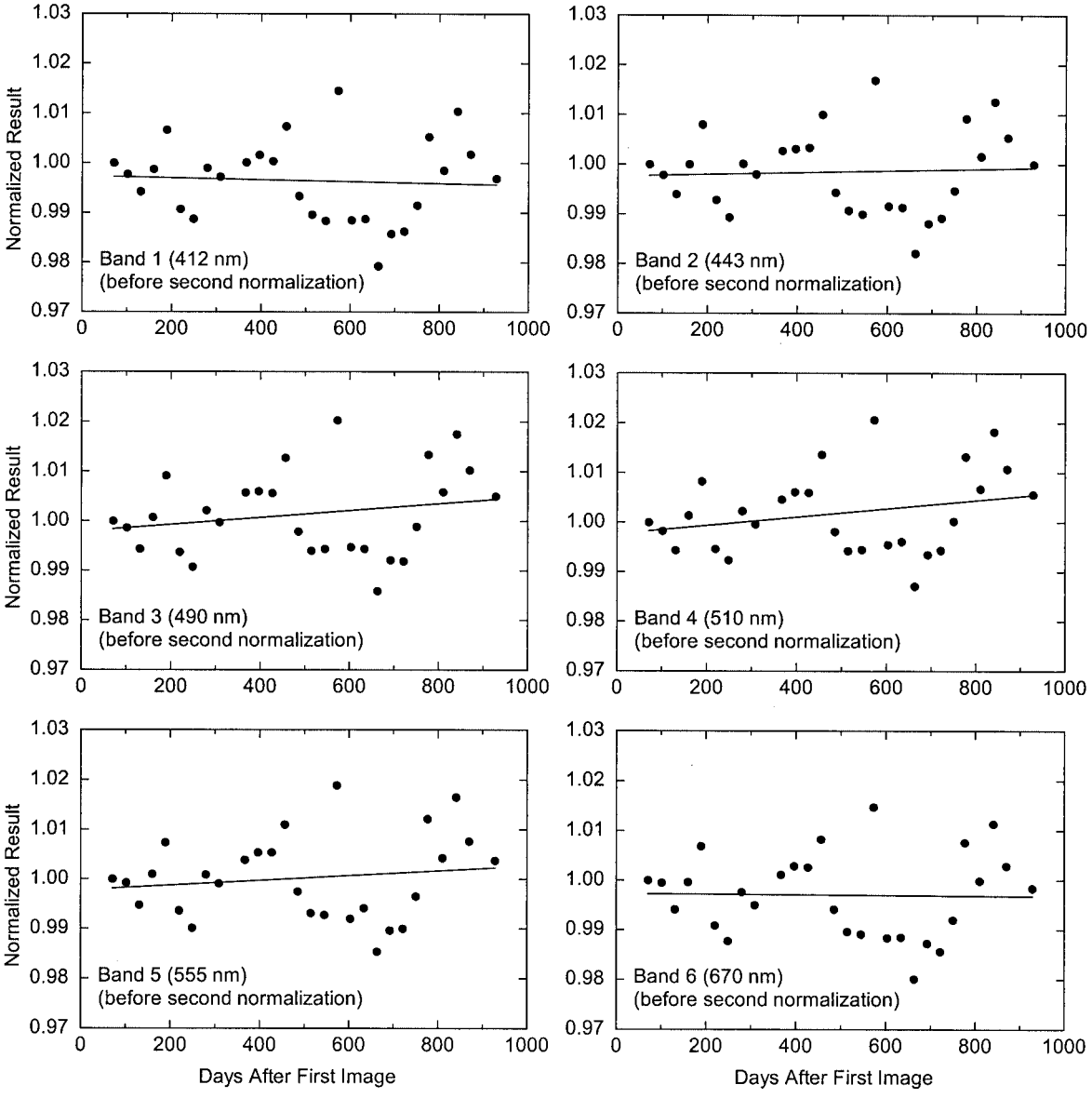

Fig. 6. Lunar-measurement results for SeaWiFS bands 1 through 6. The integrated disk radiances are normalized to unity for the first lunar measurement (on 4 November 1997). For the SeaWiFS lunar analysis, this is called the first normalization. The time series for each band has been fitted to a straight line. Although the slopes of the linear regressions differ slightly from band to band, there is a pattern in the results that repeats from measurement to measurement.

and the data in this figure have been normalized to a value of unity at the time of the first SeaWiFS image (4 September 1997), rather than at the time of the first lunar image. For each band, an extrapolation based on its fitted curve provides this normalization. The curves in Fig. 9 give the values for the time-dependent instrument changes used in the current reprocessing of SeaWiFS,[29] which occurred in May 2000. The fitted curves for bands 3 and 4 are straight lines. For bands 1, 2, 5, and 6, the fitted curves are quadratic from day 0 to day 809 and linear after that. For the processing of SeaWiFS lunar measurements to date, quadratic fits have been used as the simplest means of incorporating nonlinear changes with time.[6] For bands 7 and 8, the fitted curves are two quadratics from day 0 to 809, giving better agreement with the data, and a linear fit after that. Day 809 after launch marked the end of the analysis period before the current reprocessing of the SeaWiFS data set. Although the quadratic curves in Fig. 9 can be used to track the changes of the instrument in the past, we do not consider them adequate in predicting future instrument performance. Thus the project uses sets of linear segments to track the instrument changes between reprocessings. These segments are generally a few months long. For the next SeaWiFS reprocessing, due to occur in 2001 or 2002, the line segments after day 809 will be replaced with fitted curves.

The lunar data in Fig. 9, particularly those for band

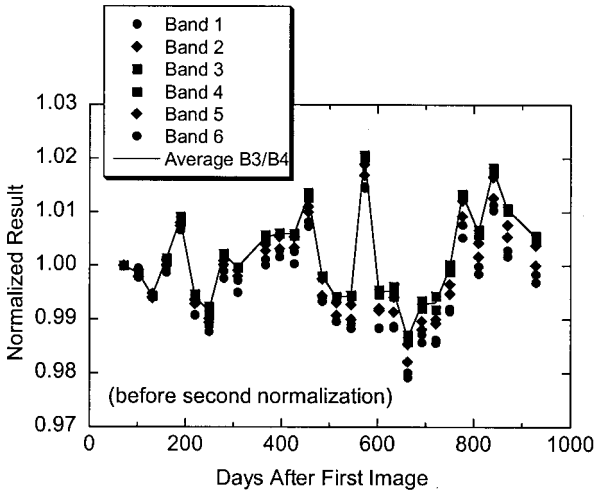

Fig. 7. Lunar measurement results for SeaWiFS bands 1 through 6. This is a compilation of the values in the panels of Fig. 5, without the linear regressions. Instead, there is a line that connects the average of the values for band 3 and band 4 for each lunar measurement. There is a spread over time in the results, with the values for bands 1 and 6 the lowest at day 930, and the values for bands 3 and 4 the highest. We know of no mechanism that improves the radiometric sensitivity of bands 3 and 4 over time, so we have assumed that the radiometric sensitivity of these bands has decreased the least (that is, not at all). As a result, we have normalized the values for all of the bands to the average of bands 3 and 4 for each lunar measurement (see Fig. 8). For the SeaWiFS lunar analysis, this is called the second normalization.

8, show cyclical oscillations for a period of one year. The current fitting scheme incorporates these oscillations into the coefficients used in Eq. (1). However, with the completion of nearly three years of measurements, it is possible to examine these oscillations more closely. Such an examination is shown in Fig. 10. In Fig. 10(a), the lunar measurements for band 8 have been fitted to a single exponential curve. The curve approaches a value of 0.885 several years into the future. It has a three-parameter fit, and when this exponential is substituted for the quadratic portion of Eq. (1), it gives the form

$$L_T = (\mathrm{DN} - \mathrm{DN}_0)[k_2(g)\alpha(t_0)(1 - \beta\{1 - \gamma \exp[-\delta(t - t_0)]\})^{-1}], \quad (13)$$

where the terms β, γ, and δ from Eq. (1) are reused. However for Eq. (13), β and γ are dimensionless, and δ has units of day^{-1}. For times far into the future, the correction term approaches a value of $(1 - \beta)$. The SeaWiFS Project is currently considering the suitability of substituting Eq. (13)–or a modified version of it–for Eq. (1) as the SeaWiFS calibration equation at the next reprocessing of the data set.

Figure 10(b) shows the differences of the band 8 lunar measurements from the fitted curve. The differences take the form of an oscillation with the high points near the time of the winter solstice, when the Earth is closest to the Sun. The low points occur near the summer solstice when the Earth–Sun distance is greatest. This oscillation correlates well with the annual cycle in the focal-plane temperature for band 8, which is also warmest near the winter solstice [see Fig. 10(c)]. Since panels 10(b) and 10(c) use the same abscissa, it is a straightforward process to plot the band 8 residual versus focal-plane temperature. This is shown in panel 10(d), along with a straight-line curve fit.

The SeaWiFS instrument model includes a focal-plane temperature factor, a dimensionless correction with a value close to unity.[12] This correction takes the form

$$T_{\mathrm{CORR}} = [1 + k_3(T - T_{\mathrm{REF}})], \quad (14)$$

where T_{CORR} is the temperature correction (dimensionless), k_3 is the correction constant (in $^\circ\mathrm{C}^{-1}$), T is the temperature (in °C), and T_{REF} is the reference temperature determined during the laboratory characterization of the instrument (20 °C). T_{CORR} is applied as a multiplicative correction to the radiances calculated using Eq. (1).[12] The term in brackets is

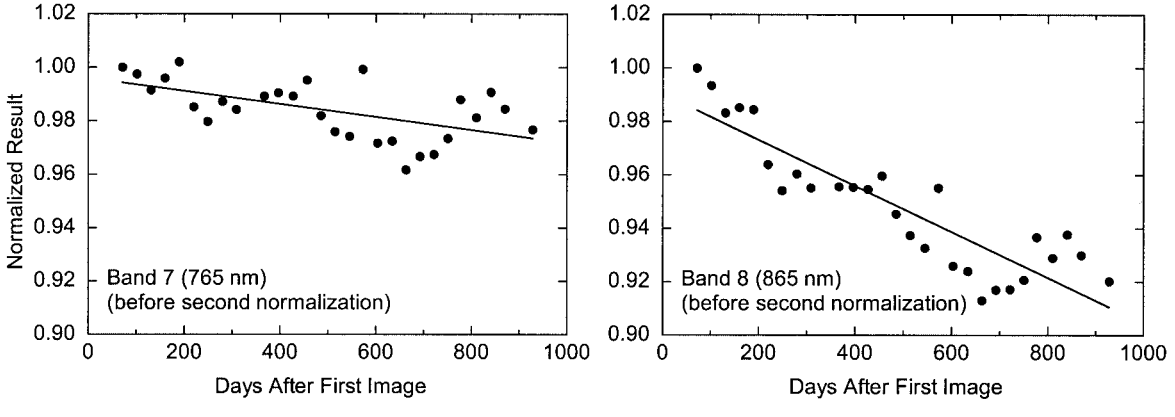

Fig. 8. Lunar measurement results for SeaWiFS bands 7 and 8. As with Fig. 5, the integrated disk radiances are normalized to unity for the first lunar measurements on 4 November 1997. The time series for each band has also been fitted to a straight line. The vertical scale for this figure is twice that for Figs. 5 and 6, so the measurement-to-measurement patterns shown here for these bands appear smaller than for bands 1–6.

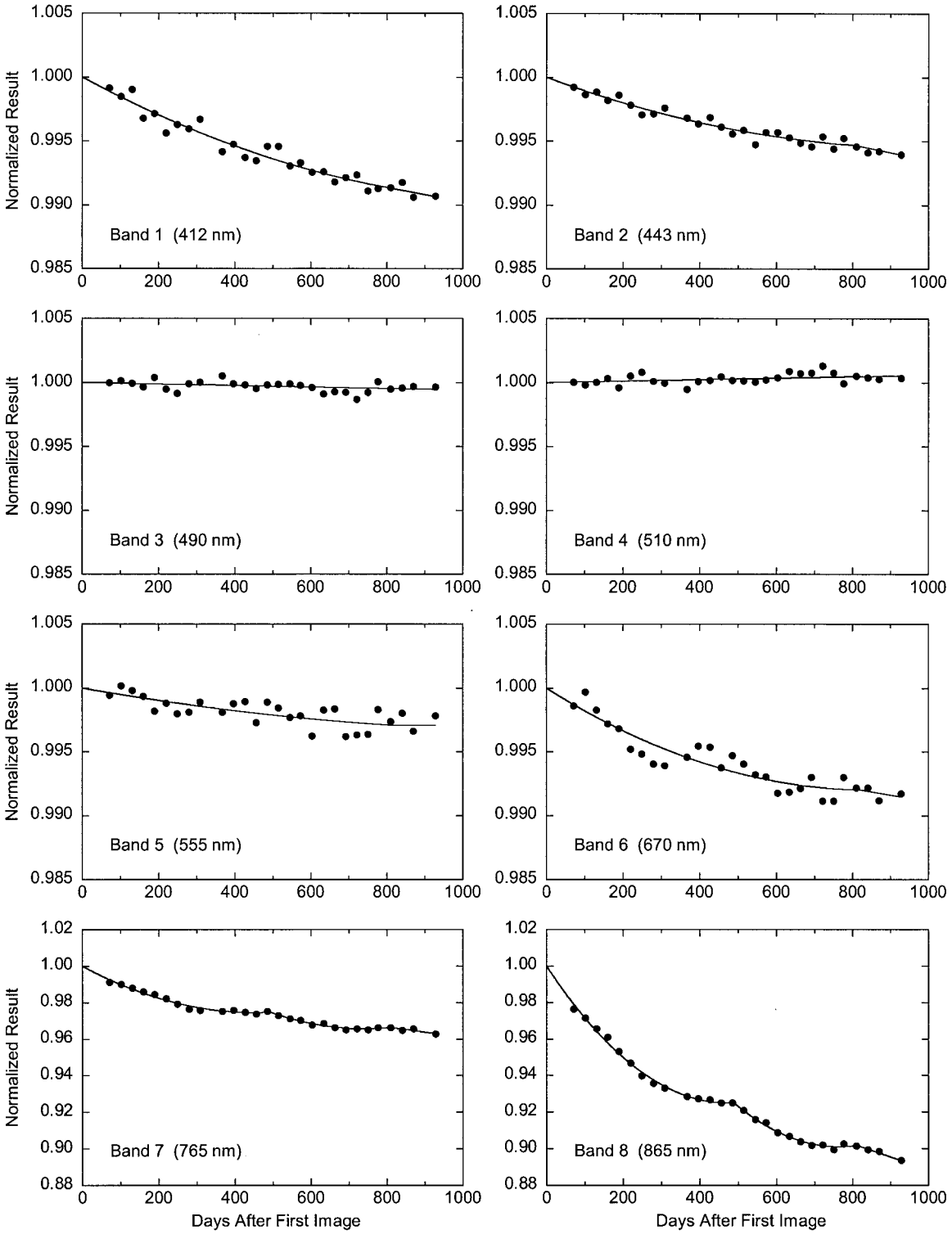

Fig. 9. Changes in the radiometric sensitivity of SeaWiFS as determined from lunar measurements. These results have been normalized to the average of bands 3 and 4 for each measurement. The fitted curves shown here give the on-orbit changes in the instrument for use in Eq. (1). The curves are combinations of straight lines and one or more quadratic functions.

unity when the temperature of the focal plane equals T_{REF} and increases with increasing temperature. This reflects the fact that for each band the output of the photodiode and its associated electronics on the focal plane decreases slightly as the focal-plane temperature increases. As shown in Eq. (1), a decrease in the SeaWiFS output ($\mathrm{DN} - \mathrm{DN}_0$) causes a decrease in the calculated radiance, $L_T(\lambda)$. As shown in Fig. 10(d), the output from SeaWiFS band 8 increases slightly with increasing focal plane temperature, in-

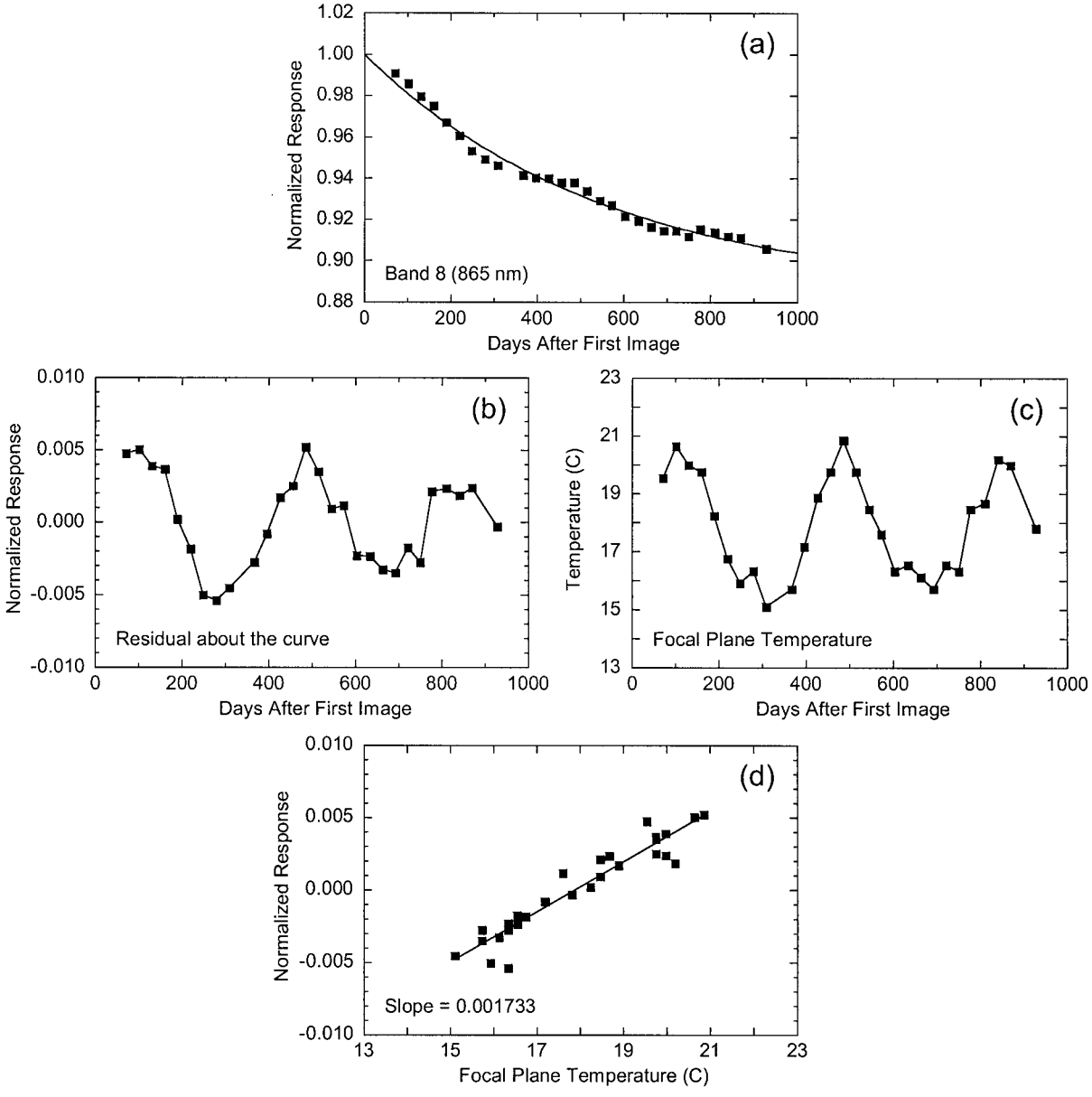

Fig. 10. Calculation of the residual temperature dependence for SeaWiFS band 8. (a) Lunar measurements for SeaWiFS band 8, plotted with a single exponential curve. The curve flattens out at a value of 0.885. (b) Residuals of the data points in panel (a) about the fitted curve. These residuals are cyclic with a period of one year. (c) Temperatures of the band 7/8 focal plane for the set of lunar measurements. The patterns of panels (b) and (c) are in phase, indicating an overcorrection for the focal-plane temperature in the instrument model. (d) Residuals about the fitted curve plotted versus focal-plane temperature. The slope in this panel gives the excess in the value for the k_3 coefficient for band 8. This is the amount that the coefficient must be reduced to minimize the oscillation in panel (b).

dicating that its focal-plane temperature factor overcorrects slightly. In other words, the current value of k_3 in the instrument model for band 8 is too large, by the amount of the slope in Fig. 10(d). For bands 1 through 6, the correlation with focal-plane temperature is lost in the scatter of the data about the trend lines.

The oscillations for bands 7 and 8 in Fig. 9 are part of the current processing of the SeaWiFS data. Those oscillations are real. They have an instrumental cause; that is, there is a problem with the instrument model for SeaWiFS. The trend lines account for them. By adjusting the focal-plane temperature factors for bands 7 and 8, it is possible to remove the cyclical pattern in the lunar time series for these bands, as shown in Fig. 11. With the next SeaWiFS reprocessing we anticipate updating our instrument model and removing these oscillations from the time series. To a certain extent, this revision to our analysis will be purely cosmetic, since it will make the time series smooth but will not improve the quality of the time-dependent correction. How-

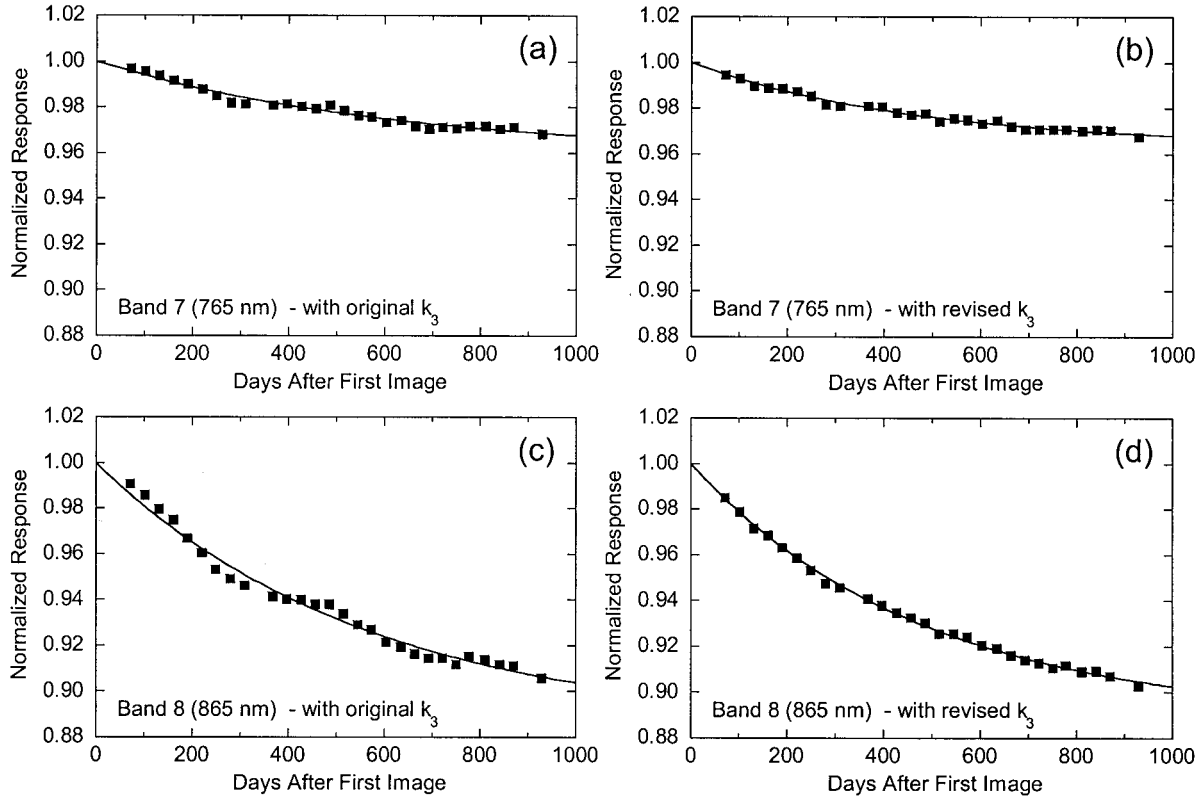

Fig. 11. Changes in the lunar measurements for bands 7 and 8. The changes derive from differences in the focal-plane temperature correction factors (k_3). The original k_3's come from Table 10 of Barnes *et al.*[12] The revised k_3's come from the procedure summarized in Fig. 6. (a) Lunar measurements from band 7 with use of the original value for k_3. (b) Lunar measurements from band 7 with use of the revised values for k_3. The fitted curve in this panel is slightly different from that in panel 7(a). (c) Lunar measurements from band 8 with use of the original value for k_3. (d) Lunar measurements from band 8 with use of the revised values for k_3. The fitted curve in this panel is slightly different from that in panel 7(c).

ever, the revision stems from an improved understanding of the operating characteristics of SeaWiFS and returns us to a simple theory for the relatively large changes in SeaWiFS bands 7 and 8 that the changes are caused by decreases in the quantum efficiencies of the photodiodes from exposure to infrared radiation on orbit. We anticipate that if this theory is correct the changes in these bands will continue to dampen with time.

D. Uncertainties

The estimated uncertainties for the calibration of SeaWiFS come from three sources: the prelaunch calibration, the transfer-to-orbit experiment, and the instrument changes derived from lunar measurements. For these sources, the uncertainties are 3%,[11] 3%,[18] and 1%, respectively. The root sum square for these uncertainties is 4.4%. For the SeaWiFS Project, the assessment of an uncertainty at the 0.1% level is considered unrealistic, so the uncertainty in the SeaWiFS top-of-the-atmosphere radiances is estimated to be 4–5%. Of particular importance is the knowledge of the changes in the radiometric sensitivity of the SeaWiFS bands. For the CZCS, the uncertainty in these changes was particularly vexing, since the derived water-leaving radiances are highly sensitive to instrumental changes. For SeaWiFS, there is no sign to date of uncorrected changes in the radiometric sensitivity in any of the instrument bands, particularly in comparisons with the water-leaving radiances provided as surface truth by the Marine Optical Buoy (MOBY).[9]

4. Validation Measurements

A. Atmospheric Correction Algorithm Overview

For each of its bands, SeaWiFS measures the top-of-the-atmosphere radiance, $L_T(\lambda)$. The atmospheric-correction algorithm accounts for all of the contributors to this radiance, except for the portion that leaves the surface of the water, $L_W(\lambda)$. To do this, the algorithm separates the top-of-the-atmosphere radiance into several components:

$$L_T(\lambda) = L_R(\lambda) + [L_A(\lambda) + L_{RA}(\lambda)] + T(\lambda)L_G(\lambda) + t(\lambda)L_{WC}(\lambda) + t(\lambda)L_W(\lambda), \quad (15)$$

where the terms $L_R(\lambda)$, $L_A(\lambda)$, and $L_{RA}(\lambda)$ are contributions, respectively, from scattering by air molecules (Rayleigh scattering), aerosols, and Rayleigh–aerosol interactions. Of these contributions, $L_R(\lambda)$ can be determined accurately with a knowledge of the

surface pressure.[30] $L_G(\lambda)$ is the contribution from sun glint, which is attenuated by the direct transmittance of the atmosphere, $T(\lambda)$. Areas where the sun glint is significant can be predicted and avoided by viewing away from the point of specular reflection. For other areas, there is a correction in the algorithm for the small effects of residual glint.[31] $L_{WC}(\lambda)$ is the upwelling radiance that arises from sunlight and skylight reflecting from whitecaps on the ocean surface. At the top of the atmosphere, $L_{WC}(\lambda)$ is attenuated by the diffuse transmittance of the atmosphere, $t(\lambda)$. The whitecap radiance can be estimated at low wind speeds,[32,33] and highly contaminated data can be avoided at higher speeds, since the wind field is part of the ancillary data products for SeaWiFS.[34] The term $t(\lambda)L_W(\lambda)$ is the top-of-the-atmosphere contribution from the water-leaving radiance. $L_W(\lambda)$ is the unknown in this equation.

The heart of the SeaWiFS atmospheric correction is the determination of the radiance from aerosol and Rayleigh–aerosol interactions, $[L_A(\lambda) + L_{RA}(\lambda)]$. Rayleigh–aerosol interactions involve sunlight that is scattered from an air molecule to an aerosol particle and then to the top of the atmosphere, plus sunlight that is scattered from an aerosol particle and then an air molecule. The determination of the aerosol contribution is made with use of Eq. (15) and a set of aerosol models. However, it cannot be made with use of the SeaWiFS visible bands, because of the water-leaving radiance $L_W(\lambda)$. For this reason, SeaWiFS uses bands at 765 and 865 nm to provide $[L_A(\lambda) + L_{RA}(\lambda)]$ for all of the wavelengths. Calculation of this term requires $L_W(\lambda)$ to be either negligibly small (the black-pixel assumption) or calculable for the near-infrared bands. For ocean waters with high chlorophyll concentrations (about 2 mg M^{-3} or greater), the surface chlorophyll in the ocean can provide a source of water-leaving radiance in the near infrared,[35] as can particulates in the water column.[36] For these reasons, the vicarious calibration of SeaWiFS in the near infrared occurs in clear, low-chlorophyll waters, minimizing the effect of water-leaving radiance. Thus for the near infrared bands Eq. (15) can be simplified to give

$$L_T(\lambda) - L_R(\lambda) - t(\lambda)L_{WC}(\lambda) = [L_A(\lambda) + L_{RA}(\lambda)], \quad (16)$$

where the top-of-the-atmosphere radiance is measured and the Rayleigh and whitecap radiances can be calculated.

Since the black-pixel assumption cannot be applied to the visible-band measurements as it can to those in the near infrared, the aerosol radiances in the visible cannot be determined directly. Thus the value of $[L_A(\lambda) + L_{RA}(\lambda)]$ must be inferred from the near-infrared measurements. This is a two-step process. First, the aerosol type is determined. For measurements around the MOBY site, band 7 is calibrated vicariously to give the appropriate radiance, relative to band 8, for the marine aerosol type known to occur at the site.[9] Associated with this aerosol type is a model that gives the single-scattering reflectances, $\rho_{AS}(\lambda)$, at the visible and near-infrared wavelengths. This model gives the scattering characteristics of the aerosol at the wavelengths for all of the SeaWiFS bands.[37] However, it does not give the amount of the aerosol in the atmosphere. In the second step, the aerosol amount is determined with SeaWiFS band 8. Using the aerosol type and the aerosol radiance at 865 nm, we can calculate $[L_A(\lambda) + L_{RA}(\lambda)]$ for the SeaWiFS visible bands, in addition to the other terms in the atmospheric correction, including the diffuse transmittance of the atmosphere $t(\lambda)$. Thus the measurements from band 8 calibration propagate throughout the data set. To date, there is no means to calibrate SeaWiFS band 8 vicariously. For the visible bands, the vicarious calibration at MOBY is applied to the "instrument/atmospheric correction algorithm system," which includes the effects of the calibration of band 8 (Ref. 9).

B. Band 8 Gain Study

The Southern Ocean study examines the top-of-the-atmosphere radiance at a location similar to the region around the MOBY site, a region with clear, nearly chlorophyll-free waters. Southern Ocean measurements can be selected that are free of sun glint and that have low wind speeds, causing low and easily calculable whitecap radiances. This allows the use of Eq. (16), which, for band 8, is given as

$$L_T(865) - L_R(865) - t(865)L_{WC}(865) = [L_A(865) + L_{RA}(865)], \quad (17)$$

where $L_T(865)$ is the top-of-the-atmosphere radiance measured by SeaWiFS, and the remaining terms are calculated by the atmospheric-correction algorithm. One additional characteristic of the ocean surrounding the Antarctic Continent is the very low concentration of atmospheric aerosols. Thus at times there are SeaWiFS measurements for which the right-hand side of Eq. (17), as calculated by the atmospheric-correction algorithm, should be very close to zero. This condition allows a check of the calibration of SeaWiFS band 8 with use of the minimum value of $[L_A(865) + L_{RA}(865)]$, which corresponds to an atmosphere with near-zero aerosols. If the minimum value for $[L_A(865) + L_{RA}(865)]$ is negative, then band 8 is miscalibrated, giving values of $L_T(865)$ that are too small. If the minimum is significantly greater than zero, then band 8 gives values of $L_T(865)$ that are too large. This miscalibration can be expressed in relative terms by dividing the minimum value by the measured top-of-the-atmosphere radiance.

For the band 8 gain study, a search has been made of SeaWiFS measurements of the Southern Ocean during the Austral summer of 1997/1998 with the criteria given above: clear waters, no sun glint, and low white caps (that is, low wind speeds). Also, the cloud threshold exclusion criterion was set well below the standard processing value to avoid any contamination by cirrus clouds, subpixel clouds, and cloud edges. From this search, the minimum value for

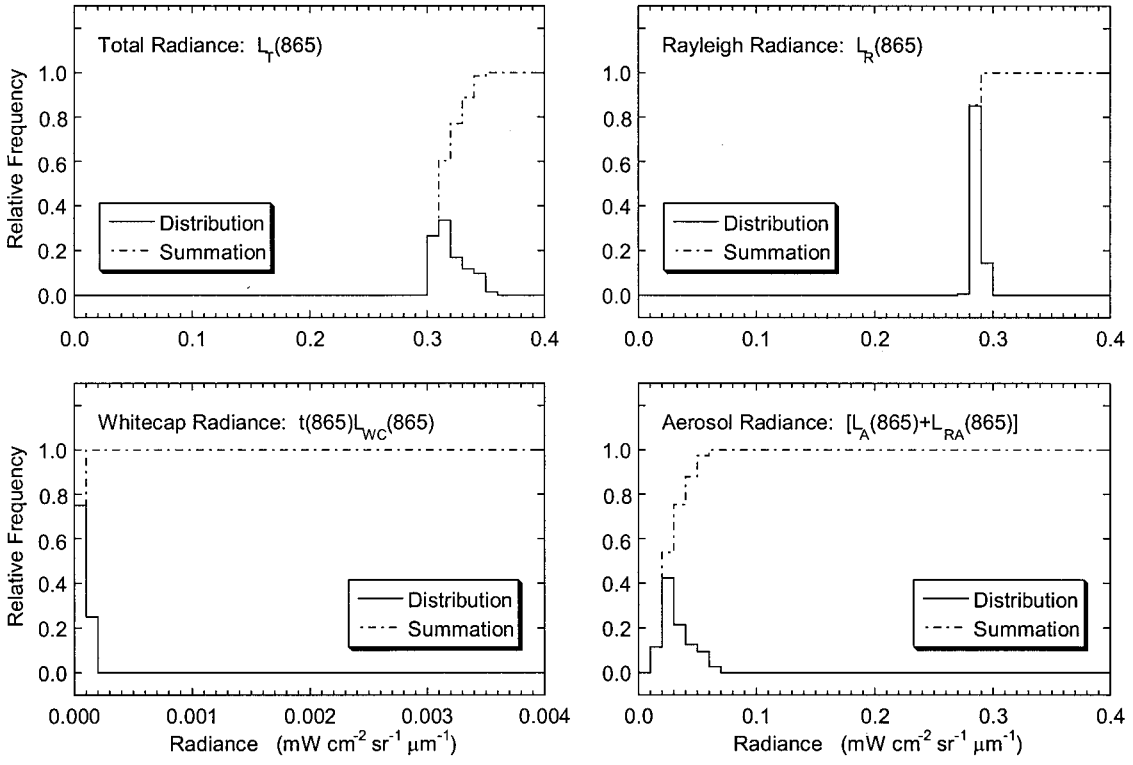

Fig. 12. Radiances from the Southern Ocean study. For the total radiances, the Rayleigh radiances, and the aerosol radiances, the results have been collected into 0.01 mW cm^{-2} sr^{-1} μm^{-1} bins. For the whitecap radiances, the bins are 100 times smaller. In addition to showing the distributions, the results have been summed to give cumulative distributions with maximum values of unity. The aerosol radiances have been calculated from the others with use of Eq. (17).

$[L_A(865) + L_{RA}(865)]$ has been found. If it is assumed that there are no atmospheric aerosols present for the measurements with these minimum values (the zero aerosol-radiance assumption), then the radiances on the right-hand side of Eq. (17) can be considered as excess radiances that result from the miscalibration of band 8. On the basis of these results, it is possible to set an upper limit for the miscalibration of the band. This can be expressed in fractional terms,

$$R_L = \frac{[L_A(865) + L_{RA}(865)]}{L_T(865)}, \qquad (18)$$

where R_L is the fractional amount of aerosol radiance calculated from the measurement. For this study, the minimum value of R_L is considered to be the maximum fractional miscalibration of band 8, since, for this value, the numerator of the ratio is assumed to contain excess radiance only. For larger values of R_L, the numerators of the ratios contain aerosol radiances in addition to the excess radiance from the miscalibration. The reason that these results give an upper limit for the miscalibration comes from the possibility that the minimum value of R_L may also include some contribution from atmospheric aerosols.

The radiances from the Southern Hemisphere study are shown in Fig. 12. There are 1235 samples in the data set. The radiances in each of the samples have been normalized to an overhead Sun using the cosine of the solar zenith angle. The cosine correction has the effect of reducing the spread in each of the distributions in Fig. 12. However, it does not affect the results of the study, since for every sample, it is applied to each term in Eq. (17) and, as a result, falls out of the ratio in Eq. (18). The distribution of the 1235 calculated values of R_L is shown in Fig. 13. The bin with the smallest values for R_L has values between 0.05 and 0.06. This contains about one-tenth of the total distribution. There are some values in the bin from 0.04 to 0.05, but these values comprise only two hundredths of the total distribution. Thus the minimum value of R_L for this study falls between 0.05 and 0.06. In other terms, the maximum fractional miscalibration of band 8 is between 5% and 6%, with the instrument producing radiances that are too large.

It is possible to check the quality of the zero aerosol-radiance assumption in the Southern Ocean. At McMurdo Station on the edge of the Antarctic continent, a Cimel sun photometer made aerosol measurements during the Austral summer of 1997/1998. The time series for early December 1997 is shown in Fig. 14. This time series has been screened to remove measurements of clouds, although the measurements with aerosol optical thicknesses of 0.10 are probably cloud measurements that survived the screening process. Aerosol optical thickness is a measure of the column amount of aero-

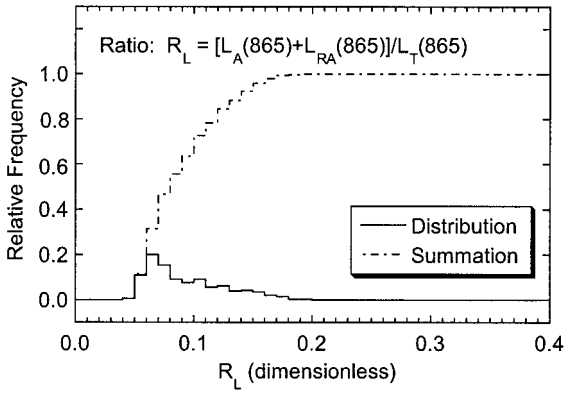

Fig. 13. Results of the Southern Ocean study. The figure gives the ratios of the aerosol radiances to the total radiances measured by SeaWiFS, calculated by use of Eq. (18). The bin with ratios from 0.05 to 0.06 contains about one-tenth of the total distribution. These are the minimum aerosol-radiance ratios for this study. If it is assumed that these minimum ratios come from measurements of an aerosol-free atmosphere, where the aerosol radiance is zero, then the radiances measured by SeaWiFS are too large by 5–6%. For the Southern Ocean study, this is the upper limit for the miscalibration of band 8.

sol in the path between the photometer and the sun. The greater the aerosol optical thickness, the greater the aerosol column amount.

For the measurements in Fig. 14, a substantial fraction of the values have aerosol optical thicknesses of 0.02 or less. These values are at or below the minimum resolution of the McMurdo Cimel, and they cannot be distinguished from measurements of an aerosol-free atmosphere. In addition, there are climatological studies[38,39] that show extremely low aerosol amounts to be common in the Antarctic. These checks of the zero aerosol-radiance assumption are important to the Southern Ocean study, since they support the hypothesis that the miscalibration of SeaWiFS band 8 is close to the 5–6% upper limit from the study. However, these measurements

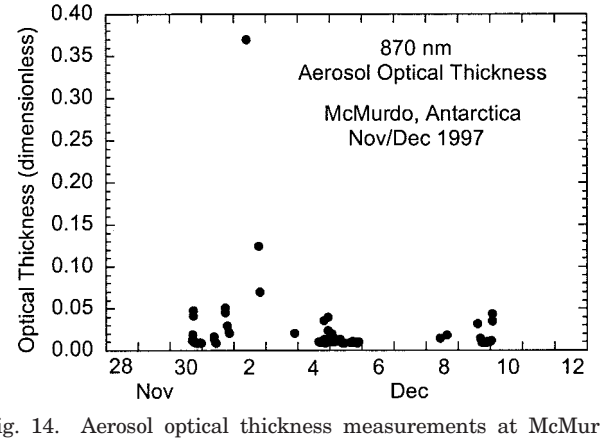

Fig. 14. Aerosol optical thickness measurements at McMurdo Station, Antarctica. For aerosol optical thicknesses of 0.02 or less, the values are at or below the minimum resolution of the instrument. They cannot be distinguished from measurements of an aerosol-free atmosphere.

were not made over the Southern Ocean itself, and this limits their usefulness. There is no evidence from these data to suggest that the calibration coefficient for SeaWiFS band 8 is too low.

C. Comparisons with Aircraft- and Ground-Based Measurements

SeaWiFS has participated in a top-of-the-atmosphere radiance comparison program that uses the NASA Airborne Visible/Infrared Imaging Spectrometer (AVIRIS)[40] as a reference. For the SeaWiFS program, the AVIRIS measurements are used to check the near-infrared bands, which are not vicariously calibrated with MOBY. For these and for other field comparisons, the vicarious calibration for SeaWiFS band 7 has not been applied. In the 1997 comparison campaign SeaWiFS radiances at 865 nm were 8.4% higher than those from AVIRIS,[41] and in the 1999 comparisons SeaWiFS was 9.0% higher. For the 765-nm SeaWiFS band, the top-of-the-atmosphere radiances were 6.2% and 6.1% higher than AVIRIS in 1997 and 1999, respectively.

The SeaWiFS Project also participates in a radiance-comparison program that uses surface measurements by the Remote Sensing Group of the University of Arizona. Initial results from this program have shown agreement between the two sets of measurements at the 10% level or better,[42] which are within the estimated uncertainties of the surface-based measurements. For two of the field campaigns, the surface and atmospheric measurements by the Remote Sensing Group provided top-of-the-atmosphere radiances at 765 and 865 nm that were 5–10% higher than those from SeaWiFS. For the third campaign, the surface-based measurements were nearly 10% lower than SeaWiFS. Currently, field measurements do not confirm the direct calibration of SeaWiFS at better than the 10% level, and at present the results from these programs are not used to adjust the SeaWiFS calibration coefficients.

5. Concluding Remarks

The SeaWiFS top-of-the-atmosphere radiances are derived from the instrument's output signals with use of the coefficients from the direct calibration of SeaWiFS, as described above. However, the principal purpose of SeaWiFS is the production of a long-term, global, ocean-color data set. For this data set, the radiances at the ocean surface are of prime importance. These radiances are combined with those from the atmosphere to provide the radiances measured by SeaWiFS, and the atmosphere contributes approximately 90% of the top-of-the-atmosphere radiance. As a result, it is the "instrument/atmospheric correction algorithm system"[4] that is vicariously calibrated to provide the best possible ocean color measurements.

SeaWiFS top-of-the-atmosphere radiances are also used to provide data products from the land surface and from clouds. This capability derives from the SeaWiFS bilinear gains described above. For these products, the atmospheric-correction algorithm is

less important, because clouds and the surface of the land are generally much brighter than the ocean. In addition, it is not possible to determine the contribution of atmospheric aerosols to the top-of-the-atmosphere radiance over these targets, as is done in the vicarious calibration of the instrument for ocean measurements. For the ocean, the water-leaving radiance is small in the near infrared,[35] allowing for measurements of light from the atmosphere alone. For land measurements, the near-infrared surface radiance can be very large, contaminating the radiances that could be used to determine aerosol type and amount. Because of these factors, the vicarious calibration at MOBY is not applied to SeaWiFS land and cloud measurements. And for these measurements, SeaWiFS provides no information on atmospheric aerosols.

The SeaWiFS Project has developed a partial atmospheric correction for land measurements that calculates the Rayleigh component of the upwelling radiance, including a surface pressure dependence for each SeaWiFS band. Along with this correction, the SeaWiFS Project has incorporated algorithms to provide land surface properties,[43] using the normalized difference vegetation index and the enhanced vegetation index. In addition, an algorithm has been developed to produce surface reflectances. Each of these algorithms uses SeaWiFS top-of-the-atmosphere radiances determined by the direct calibration of the instrument. To date, there is no vicarious calibration for SeaWiFS measurements of the land surface or of clouds.

The authors thank the two anonymous reviewers for their time and effort. Their comments have improved this paper significantly. This work was conducted as part of the SeaWiFS calibration and validation program under NASA contract NAS5-00141.

References

1. W. A. Hovis, D. K. Clark, F. Anderson, R. W. Austin, W. H. Wilson, E. T. Baker, D. Ball, H. R. Gordon, J. L. Mueller, S. Z. El-Sayed, B. Sturm, R. C. Wrigley, and C. S. Yentsch, "Nimbus-7 Coastal Zone Color Scanner: system description and initial imagery," Science **210,** 60–62 (1980).
2. S. B. Hooker, W. E. Esaias, G. C. Feldman, W. W. Gregg, and C. R. McClain, *An Overview of SeaWiFS Ocean Color*, NASA Tech. Memo. 104566 **1,** S. B. Hooker and E. R. Firestone, eds. (NASA Goddard Space Flight Center, Greenbelt, Md., 1992).
3. C. R. McClain, W. E. Esaias, W. Barnes, B. Guenther, D. Endres, S. B. Hooker, B. G. Mitchell, and R. Barnes, *SeaWiFS Calibration and Validation Plan*, NASA Tech. Memo. 104566 **3,** S. B. Hooker and E. R. Firestone, eds. (NASA Goddard Space Flight Center, Greenbelt, Md., 1992).
4. R. H. Evans, and H. R. Gordon, "Coastal Zone Color Scanner 'system calibration': a retrospective examination," J. Geophys. Res. **99,** 7293–7307 (1994).
5. H. R. Gordon, "Calibration requirements and methodology for remote sensors viewing the ocean in the visible," Remote Sens. Environ. **22,** 103–126 (1987).
6. R. A. Barnes, R. E. Eplee Jr., F. S. Patt, and C. R. McClain, "Changes in the radiometric sensitivity of SeaWiFS determined from lunar and solar-based measurements," Appl. Opt. **38,** 4649–4664 (1999).
7. R. A. Barnes, W. L. Barnes, W. E. Esaias, and C. R. McClain, *Prelaunch Acceptance Report for the SeaWiFS Radiometer*, NASA Tech. Memo. 104566 **22,** S. B. Hooker, E. R. Firestone, and J. G. Acker, eds. (NASA Goddard Space Flight Center, Greenbelt, Md., 1994).
8. R. A. Barnes and A. W. Holmes, "Overview of the SeaWiFS ocean sensor," in *Sensor Systems for the Early Earth Observing System Platforms*, W. L. Barnes, ed., Proc. SPIE **1939,** 224–232 (1993).
9. R. E. Eplee, Jr., W. D. Robinson, S. W. Bailey, D. K. Clark, P. J. Werdell, M. Wang, R. A. Barnes, and C. R. McClain, "The calibration of SeaWiFS. II. vicarious techniques," Appl. Opt. **40,** 6701–6718 (2001).
10. R. A. Barnes, "SeaWiFS data: actual and simulated," (NASA Goddard Space Flight Center, Greenbelt, Md., 1994), from http://seawifs.gsfc.nasa.gov/SEAWIFS/IMAGES/spectra1.dat and /spectra2.dat.
11. B. C. Johnson, E. A. Early, R. E. Eplee Jr., R. A. Barnes, and R. T. Caffrey, *The 1997 Prelaunch Calibration of SeaWiFS*, NASA Tech. Memo. 1999-206892 **4,** S. B. Hooker and E. R. Firestone, eds. (NASA Goddard Space Flight Center, Greenbelt, Md., 1999).
12. R. A. Barnes, A. W. Holmes, W. L. Barnes, W. E. Esaias, C. R. McClain, and T. Svitek, *SeaWiFS Prelaunch Radiometric Calibration and Spectral Characterization*, NASA Tech. Memo. 104566 **23,** S. B. Hooker, E. R. Firestone and J. G. Acker, eds. (NASA Goddard Space Flight Center, Greenbelt, Md., 1994).
13. R. A. Barnes, and R. E. Eplee Jr., "The 1993 SeaWiFS calibration using band-averaged spectral radiances," in *SeaWiFS Calibration Topics, Part 2*, NASA Tech. Memo. 104566 **40,** S. B. Hooker and E. R. Firestone, eds. (NASA Goddard Space Flight Center, Greenbelt, Md., 1997) pp. 39–47.
14. E. A. Early, and B. C. Johnson, "Calibration and characterization of the GSFC sphere," in *Case Studies for SeaWiFS Calibration and Validation, Part 4*, NASA Tech. Memo. 104566 **41,** S. B. Hooker and E. R. Firestone, eds. (NASA Goddard Space Flight Center, Greenbelt, Md., 1997) pp. 3–17.
15. B. C. Johnson, J. B. Fowler, and C. R. Cromer, *The SeaWiFS Transfer Radiometer* (*SXR*), NASA Tech. Memo. 1998-206892 **1,** S. B. Hooker and E. R. Firestone, eds. (NASA Goddard Space Flight Center, Greenbelt, Md., 1998).
16. R. A. Barnes, A. W. Holmes, and W. E. Esaias, *Stray Light in the SeaWiFS Radiometer*, NASA Tech. Memo. 104566 **31,** S. B. Hooker, E. R. Firestone, and J. G. Acker, eds. (NASA Goddard Space Flight Center, Greenbelt, Md., 1995).
17. E-n. Yeh, M. Darzi, and L. Kumar, "SeaWiFS stray light algorithm," in *Case Studies for SeaWiFS Calibration and Validation, Part 4*, NASA Tech. Memo. 104566 **41,** S. B. Hooker and E. R. Firestone, eds. (NASA Goddard Space Flight Center, Greenbelt, Md., 1997) pp. 24–30.
18. R. A. Barnes, R. E. Eplee, Jr., S. F. Biggar, K. J. Thome, E. F. Zalewski, P. N. Slater, and A. W. Holmes, "SeaWiFS transfer-to-orbit experiment," Appl. Opt. **39,** 5620–5631 (2000).
19. R. A. Barnes, and R. E. Eplee, Jr., "The SeaWiFS solar diffuser," in *SeaWiFS Calibration Topics, Part 1*, NASA Tech. Memo. 104566 **39,** S. B. Hooker and E. R. Firestone, eds. (NASA Goddard Space Flight Center, Greenbelt, Md., 1996) pp. 54–61.
20. H. R. Gordon, "Remote sensing of ocean color: a methodology for dealing with broad spectral bands and significant out-of-band response," Appl. Opt. **34,** 8363–8374 (1995).
21. M. Wang, "A sensitivity study of the SeaWiFS atmospheric correction algorithm: effects of spectral band variations," Remote Sens. Environ. **67,** 348–359 (1999).
22. R. A. Barnes, R. E. Eplee, Jr., and F. S. Patt, "SeaWiFS measurements of the moon," in *Sensors, Systems, and Next Gen-*

eration Satellites II, H. Fujisada, ed., Proc. SPIE **3498,** 311–324 (1998).
23. R. A. Barnes and C. R. McClain, "The calibration of SeaWiFS after two years on orbit," in *Sensors, Systems, and Next Generation Satellites III*, H. Fujisada, ed., Proc. SPIE **3870,** 214–227 (1999).
24. H. H. Kieffer and R. L. Wildey, "Establishing the moon as a spectral radiance standard," J. Atmos. Ocean. Technol. **13,** 360–375 (1996).
25. H. H. Kieffer and J. M. Anderson, "Use of the moon for spacecraft calibration," in *Sensors, Systems, and Next Generation Satellites II*, H. Fujisada, ed., Proc. SPIE **3498,** 325–336 (1998).
26. H. H. Kieffer, J. M. Anderson, and K. J. Becker, "Radiometric calibration of spacecraft using lunar images," in *Sensors, Systems, and Next Generation Satellites III*, H. Fujisada, ed., Proc. SPIE **3870,** 193–205 (1999).
27. B. Hapke, *Theory of Reflectance and Emittance Spectroscopy* (Cambridge U. Press, New York, 1993).
28. P. Helfenstein and J. Veverka, "Photometric properties of lunar terrains derived from Hapke's equations," Icarus **72,** 342–357 (1987).
29. R. E. Eplee, Jr. and R. A. Barnes, "Lunar data analysis for SeaWiFS calibration," in *SeaWiFS Postlaunch Calibration and Validation Analyses, Part 1*, NASA Tech. Memo. 2000-206892 **9,** S. B. Hooker and E. R. Firestone, eds. (NASA Goddard Space Flight Center, Greenbelt, Md., 2000) pp. 17–27.
30. H. R. Gordon, J. W. Brown, and R. H. Evans, "Exact Rayleigh scattering calculations for use with the Nimbus-7 Coastal Zone Color Scanner," Appl. Opt. **27,** 862–871 (1988).
31. M. Wang and S. W. Bailey, "Correction of the sunglint contamination on the SeaWiFS aerosol optical thickness retrievals," in *SeaWiFS Postlaunch Calibration and Validation Analyses, Part 1*, NASA Tech. Memo. 2000-206892 **9,** S. B. Hooker and E. R. Firestone, eds. (NASA Goddard Space Flight Center, Greenbelt, Md., 2000) pp. 64–68.
32. K. D. Moore, K. J. Voss, and H. R. Gordon, "Spectral reflectance of whitecaps: their contribution of water-leaving radiance," J. Geophys. Res. **105,** 6493–6499 (2000).
33. W. D. Robinson, G. M. Schmidt, C. R. McClain, and P. J. Werdell, "Changes made in the operational SeaWiFS processing," in *SeaWiFS Postlaunch Calibration and Validation Analyses, Part 2*, NASA Tech. Memo. 2000-206892 **10,** S. B. Hooker and E. R. Firestone, eds. (NASA Goddard Space Flight Center, Greenbelt, Md., 2000) pp. 12–28.
34. B. D. Schieber and J. K. Firestone, "The generation of CZCS ancillary data sets for simulated SeaWiFS processing," in *Case Studies for SeaWiFS Calibration and Validation, Part 2*, NASA Tech. Memo. 104566 **19,** S. B. Hooker and E. R. Firestone, eds. (NASA Goddard Space Flight Center, Greenbelt, Md., 1996).
35. D. A. Siegel, M. Wang, S. Maritorena, and W. Robinson, "Atmospheric correction of satellite ocean color imagery: the black pixel assumption," Appl. Opt. **39,** 3582–3591 (2000).
36. B. Chen, K. Stamnes, B. Yan, Ø. Frette, and J. J. Stamnes, "Water-leaving radiance in the NIR spectral region and its effects on the atmospheric correction of ocean color imagery," J. Adv. Mar. Sci. Tech. Soc. **4,** 329–338 (1998).
37. M. Wang, "The SeaWiFS atmospheric correction algorithm updates," in *SeaWiFS Postlaunch Calibration and Validation Analyses, Part 1*, NASA Tech. Memo. 2000-206892 **9,** S. B. Hooker and E. R. Firestone, eds. (NASA Goddard Space Flight Center, Greenbelt, Md., 2000).
38. G. E. Shaw, "Atmospheric turbidity in the polar regions," J. App. Meterol. **21,** 1080–1088 (1982).
39. A. Herber, L. W. Thomason, V. F. Radionov, and U. Leiterer, "Comparison of trends in the tropospheric and stratospheric aerosol optical depths in the Antarctic," J. Geophys. Res. **98,** 18441–18447 (1993).
40. W. M. Porter and H. T. Enmark, "A system overview of the Airborne Visible/Infrared Imaging Spectrometer (AVIRIS)," in *Imaging Spectroscopy II*, G. Vane, ed., Proc. SPIE **834,** 22–31 (1987).
41. R. Green and T. G. Chrien, "High altitude measurements of radiance at high spectral and spatial resolution for SIMBIOS sensor calibration, validation, and intercomparisons," in *SIMBIOS Project 1998 Annual Report*, NASA Tech. Memo. 1999-208645, C. R. McClain and G. S. Fargion, eds. (NASA Goddard Space Flight Center, Greenbelt, Md., 1999).
42. E. E. Whittington, K. J. Thome, R. A. Barnes, and K. A. Canham, "Radiometric calibration of the Sea-viewing Wide Field of View Sensor using ground-reference techniques," in *Earth Observing Systems V*, W. L. Barnes, ed., Proc. SPIE **4135,** 294–301 (2000).
43. M. J. Behrenfield, J. T. Randerson, C. R. McClain, G. C. Feldman, S. O. Los, C. J. Tucker, P. G. Falkowski, C. B. Field, R. Frouin, W. E. Esaias, D. D. Kolber, and N. H. Pollack, "Biospheric primary production during an ENSO transition," Science **291,** 2594–2597 (2001).